Linear Circuit Models of PWM Flyback and Buck/Boost Converters

Article *in* IEEE Transactions on Circuits and Systems I Fundamental Theory and Applications · September 1992

DOI: 10.1109/81.168931 · Source: IEEE Xplore

2 authors:

Dariusz Czarkowski
New York University
175 PUBLICATIONS **5,160** CITATIONS
SEE PROFILE

Marian Kazimierczuk
Wright State University
498 PUBLICATIONS **15,475** CITATIONS
SEE PROFILE

complex polynomials'," *IEEE Trans. Circuits Syst.*, vol. 38, pp. 1397–1400, Nov. 1991.

[18] H. Bouguerra, B. C. Chang, H. H. Yeh, and S. S. Banda, "Fast stability checking for the convex combination of stable polynomials," *IEEE Trans. Automat. Contr.*, vol. 35, pp. 586–588, May 1990.

Linear Circuit Models of PWM Flyback and Buck/Boost Converters

Dariusz Czarkowski and Marian K. Kazimierczuk

***Abstract*—A new method of modeling PWM converters operating in continuous conduction mode (CCM) is introduced. The procedure of deriving the models consists of three steps. First, static voltage and current transfer functions of the idealized switching part of the converters are found. Second, the linearization of these transfer functions at the operating point is carried out and the idealized switching part is replaced by dependent current and voltage sources. Third, the equivalent average resistance (EAR) of parasitic resistances and equivalent average voltage (EAV) of offset voltage sources of switches are determined using the *principle of energy conservation*. The method leads to linear dc and small-signal circuit models of a PWM converter. The obtained models give the same dc and small-signal characteristics as the state-space averaging method. To illustrate the method, the analysis of the PWM flyback converter is given, taking into account parasitic resistances of the transformer, the filter capacitor, the switch, and the diode as well as the diode threshold voltage. Design equations for dc voltage transfer function, efficiency, and small-signal characteristics are derived.**

I. Introduction

PWM dc/dc switch-mode converters are usually modeled using the state-space averaging technique and linearization [1]–[5]. This method of modeling is quite laborious, especially when the equivalent circuit contains a large number of components. To overcome this problem, linear circuit models of converters have been discussed in [6], [7]. Interesting nonlinear design techniques have been reported in [8]–[10]. However, a systematic method for including parasitic components into averaged models has not been presented.

The purpose of this paper is to introduce a simple method of obtaining dc and small-signal linear models of PWM dc/dc converters, taking into account parasitic resistances of reactive components and power switches and offset voltages of power switches. A comprehensive analysis of the PWM flyback converter is given to illustrate the new method.

II. Analysis of Flyback Converter

A circuit of the flyback converter is shown in Fig. 1(a). It is comprised of a controllable switch S (e.g., MOSFET), a transformer with a turns ratio n, a diode $D1$, a filter capacitor C, and a load resistance R. The switch is turned on and off at the switching frequency $f_s = 1/T$ with the ON duty ratio $D = t_{on}/T$, where t_{on} is the interval when the switch is ON. Fig. 1(c) depicts an equivalent circuit of the converter, where r_{DS} is the transistor ON resistance, r_{T1} is the winding resistance of the primary of the transformer, r_L is the magnetic core series resistance, L is the magnetizing inductance of the transformer, r_{T2} is the winding resistance of the secondary of the transformer, V_F is the threshold voltage of the diode, R_F is the forward resistance of the diode, and r_C is the equivalent series resistance (ESR) of the filter capacitor.

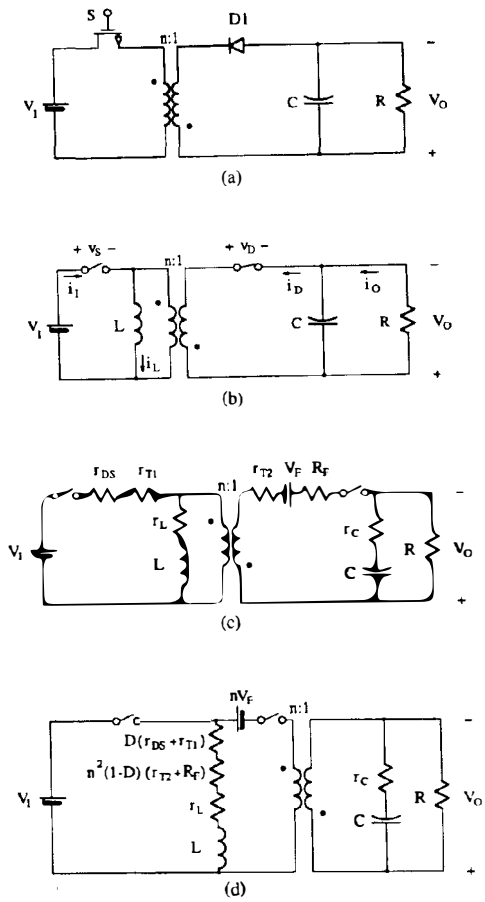

Fig. 1. PWM flyback converter. (a) Circuit. (b) Equivalent circuit with ideal components. (c) Equivalent circuit with actual components. (d) Equivalent circuit with equivalent averaged resistances connected in series with the magnetizing inductance of the transformer.

A. Assumptions

The analysis of the flyback converter of Fig. 1(a) begins with the following assumptions.

1) The power MOSFET in the ON state is modeled by a constant resistance r_{DS} and in the OFF state by an infinite resistance. Its output capacitance and lead inductance (and thereby switching losses) are zero.
2) The diode in the ON state is modeled by a constant-voltage battery V_F and a constant forward resistance R_F and in the OFF state by an infinite resistance. The charge-carrier lifetime is zero for $p-n$ junction diodes (and therefore switching losses due to the reverse recovery are zero), the diode junction capacitance and lead inductance are zero.
3) The transformer leakage inductances and the stray capacitances are neglected.

Manuscript received October 4, 1991; revised May 15, 1992. This work was supported by the National Science Foundation under Grant ECS-8922695. This paper was recommended by Associate Editor F. Y. Chang.

The authors are with the Department of Electrical Engineering, Wright State University, Dayton, OH 45435.

IEEE Log Number 9203653.

4) Passive components are linear, time-invariant, and frequency-independent.
5) The output impedance of the input voltage source is zero for both dc and ac components.
6) The ac current ripple on the dc current I_L through the primary of the transformer is negligibly small.
7) The frequencies of ac components of the input voltage and the duty cycle are lower than one-half the switching frequency, similarly as for the state-space averaging method [2], [3].

B. dc and Small-Signal Circuit Models of Flyback Converter

From the steady-state analysis, the dc voltage and current transfer functions of the idealized switching part of the converter shown in Fig. 1(b) are [2]–[4]

$$M_V \equiv \frac{V_D}{V_S} = \frac{V_O}{V_S} = \frac{D}{n(1-D)} \tag{1}$$

$$M_I \equiv \frac{I_D}{I_I} = \frac{n(1-D)}{D} \tag{2}$$

where V_S is the dc component of the voltage across the ideal switch, V_D is the dc component of the voltage across the ideal diode and is equal to V_O, I_D is the dc component of the current through the diode $D1$ equal to the dc output current I_O, and I_I is the dc component of the input current.

The total instantaneous quantities of the converter can be presented as the sum of the dc and ac components

$$v_I = V_I + v_i \tag{3}$$

$$i_I = I_I + i_i \tag{4}$$

$$v_S = V_S + v_s \tag{5}$$

$$d_{\mathrm{TOT}} = D + d \tag{6}$$

$$i_D = I_D + i_d \tag{7}$$

$$v_O = V_O + v_o. \tag{8}$$

The magnitudes of the ac components are assumed to be much lower than the dc components.

From (1) and (2),

$$v_O = M_V v_S = \frac{d_{\mathrm{TOT}}}{n(1-d_{\mathrm{TOT}})} v_S \tag{9}$$

$$i_D = M_I i_I = \frac{n(1-d_{\mathrm{TOT}})}{d_{\mathrm{TOT}}} i_I. \tag{10}$$

Substitution of (5), (6), and (8) into (9) yields

$$(D+d)(V_S + v_s) = n(1-D-d)(V_O + v_o) \tag{11}$$

which can be rearranged using (1) to the form

$$V_S + v_s + \frac{1}{D} v_s d = \frac{n(1-D)}{D} V_O + \frac{n(1-D)}{D} v_o - \frac{nV_O}{D^2} d - \frac{n}{D} v_o d. \tag{12}$$

Likewise, substituting (4), (6), and (7) into (10), one obtains

$$(D+d)(I_D + i_d) = n(1-D-d)(I_I + i_i) \tag{13}$$

from which (and (2))

$$I_D + i_d + \frac{1}{D} i_d d = \frac{n(1-D)}{D} I_I + \frac{n(1-D)}{D} i_i - \frac{nI_I}{D^2} d - \frac{n}{D} i_i d. \tag{14}$$

An equivalent averaged resistance (EAR) of the switched resistances can be determined using the *principle of energy conservation*. This concept is analogous to the equivalent averaged resistance of a switched capacitor in switched-capacitor filters. The dc component of the inductor current I_L is taken as a reference current. The switch S is ON for the interval $0 < t \le DT$ and OFF for $DT < t \le T$. The instantaneous switch current in the circuit of Fig. 1(c) is $i_I \approx I_L$, for $0 < t \le DT$, resulting in the RMS value of the switch current

$$I_{I\,\mathrm{rms}} = \sqrt{\frac{1}{T}\int_0^T i_I^2\, dt} = \sqrt{D}\, I_L. \tag{15}$$

The power dissipated in the resistor r_{DS}

$$P_{rs} = I_{I\,\mathrm{rms}}^2 r_{DS} = D r_{DS} I_L^2 \tag{16}$$

is equal to the power dissipated in the equivalent averaged resistance r_{sav} of r_{DS}

$$P_{rsav} = r_{sav} I_L^2 \tag{17}$$

resulting in the EAR of r_{DS}

$$r_{sav} = D r_{DS}. \tag{18}$$

Likewise, the EAR of r_{T1} is

$$r_{T1av} = D r_{TS}. \tag{19}$$

The diode is ON for the interval $DT < t \le T$ during which its current is $i_D \approx nI_L$, for $DT < t \le T$. The EAR of the diode forward resistances R_F is obtained in an analogous manner and is given by

$$r_F = n^2(1-D) R_F. \tag{20}$$

Similarly, the EAR of r_{T2} is

$$r_{T2av} = n^2(1-D) r_{T2}. \tag{21}$$

The same approximation of the EAR's is achieved by determining the RMS values of the currents through the resistances using trapezoidal switch and diode current waveforms.

Connecting the EAR's in series with the magnetizing inductance and transferring V_F to the primary of the ideal transformer leads to an equivalent circuit of Fig. 1(d).

Since the ac components were assumed to be much smaller than the dc components, a linear circuit model of the converter for dc and small-signal operation can be obtained by neglecting the products $v_o d$ and $i_i d$ in (12) and (14). This model is shown in Fig. 2(a). Since the voltage across the filter capacitor is constant during the time interval $(1-D)T$, the average inductance current I_L flows through the parallel combination of r_C and R during the time interval DT, resulting in the resistance connected in series with the diode

$$r_R = D(r_C \| R). \tag{22}$$

Hence, the EAR of r_R is

$$r_{Rav} = n^2 D(1-D) r_R. \tag{23}$$

Therefore, the overall EAR in series with the magnetizing inductance L is

$$\begin{aligned} r &= r_L + r_{sav} + r_{T1av} + r_F + r_{T2av} + r_{Rav} \\ &= r_L + D(r_{DS} + r_{T1}) + n^2(1-D)(R_F + r_{T2}) \\ &\quad + n^2 D(1-D)(r_c \| R). \end{aligned} \tag{24}$$

Because the model depicted in Fig. 2(a) is linear, the principle of

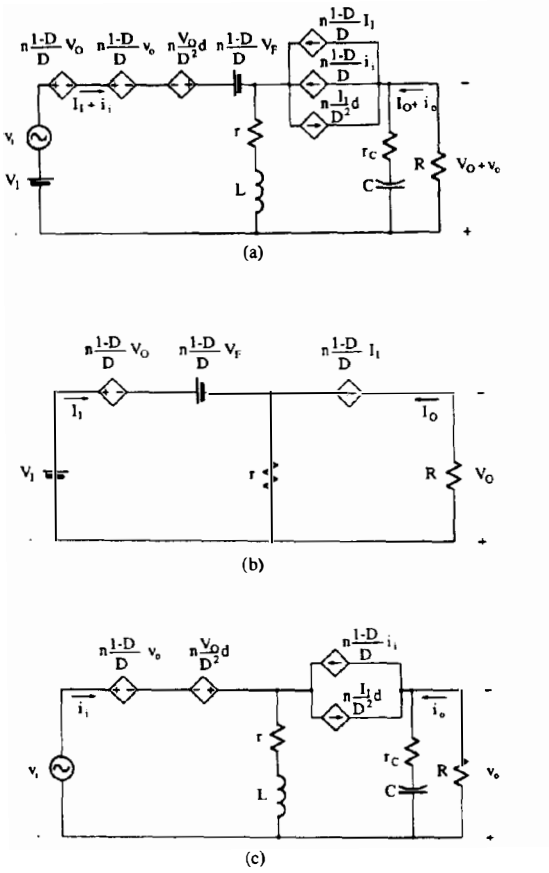

Fig. 2. Model of the flyback converter for CCM. (a) Averaged model for dc and small-signal operation. (b) dc model. (c) Small-signal model.

superposition can be used to derive a dc model shown in Fig. 2(b) and a small-signal model shown in Fig. 2(c). The important advantage of the models of Fig. 2 is that they contain standard circuit elements and therefore can be analyzed using circuit simulation programs.

Referring to Fig. 2(c), $v_o = 0$ if $[n(1-D)/D]i_i = (n/D^2)I_l d$. Accordingly, the control law is $d = (1-D)(i_i/I_l)$.

The dc model of Fig. 2(b) leads to the dc voltage transfer function

$$M_{VDC} \equiv \frac{V_O}{V_I} = \frac{nRD(1-D)}{rD[n(1-D)+D] + R[n(1-D)]^2\left(1+\frac{V_F}{V_O}\right)}. \tag{25}$$

The efficiency of the converter is found from (2) and (25) as

$$\eta \equiv \frac{V_O I_O}{V_I I_I} = \frac{V_O I_D}{V_I I_I} = M_{VDC} M_I = \frac{n(1-D)M_{VDC}}{D} = \frac{R[n(1-D)]^2}{rD[n(1-D)+D] + R[n(1-D)]^2\left(1+\frac{V_F}{V_O}\right)}. \tag{26}$$

According to the assumptions, this expression does not take into account the conduction losses caused by the ac components of currents and switching losses, similarly as the state-space averaging method. Fig. 3 shows plots of M_{VDC} and η as functions of D for different values of R for $V_O = 28$ V, $n = 5$, $r_L = 2\ \Omega$, $r_{DS} = 0.5\ \Omega$, $r_{T1} = 50$ mΩ, $V_F = 0.7$ V, $R_F = 25$ mΩ, and $r_{T2} = 10$ mΩ. These parameters are for the converter designed in the Appendix.

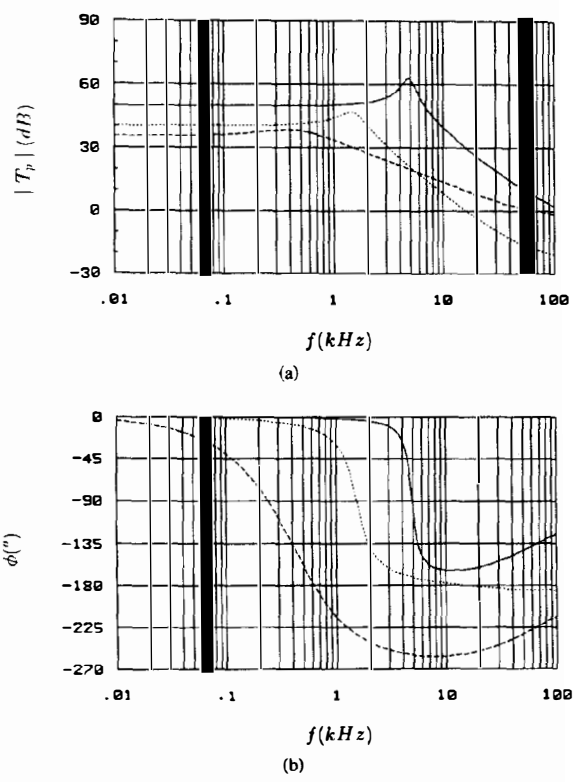

Fig. 3. dc voltage transfer function M_{VDC} and efficiency η as functions of the on duty cycle D at $R = 14$, 28, and 140 Ω for $V_F = 0.7$ V, $V_O = 28$ V, $n = 5$, $r_L = 2\ \Omega$, $r_{DS} = 0.5\ \Omega$, $r_{T1} = 50$ mΩ, $r_{T2} = 10$ mΩ, $R_F = 25$ mΩ, and $r_C = 50$ mΩ. (a) M_{VDC} versus D. (b) η versus D.

C. Small-Signal Characteristics

The small-signal dynamic characteristics of the flyback converter can be derived using the small-signal model of Fig. 2(c). They are valid for frequencies f up to about one-half the switching frequency f_s. They will be plotted for the converter designed in the Appendix.

The *control-to-output* (or *duty ratio-to-output*) *transfer function* in the s-domain is

$$T_p(s) \equiv \left.\frac{v_o(s)}{d(s)}\right|_{v_i(s)=0} = -\frac{V_O r_C}{[n(1-D)+D](1-D)(R+r_C)} \cdot \frac{(s+\omega_{tc})(s+\omega_{tl})}{s^2 + 2\xi_t\omega_t s + \omega_t^2} \tag{27}$$

where

$$\omega_{tc} = \frac{1}{Cr_C} \tag{28}$$

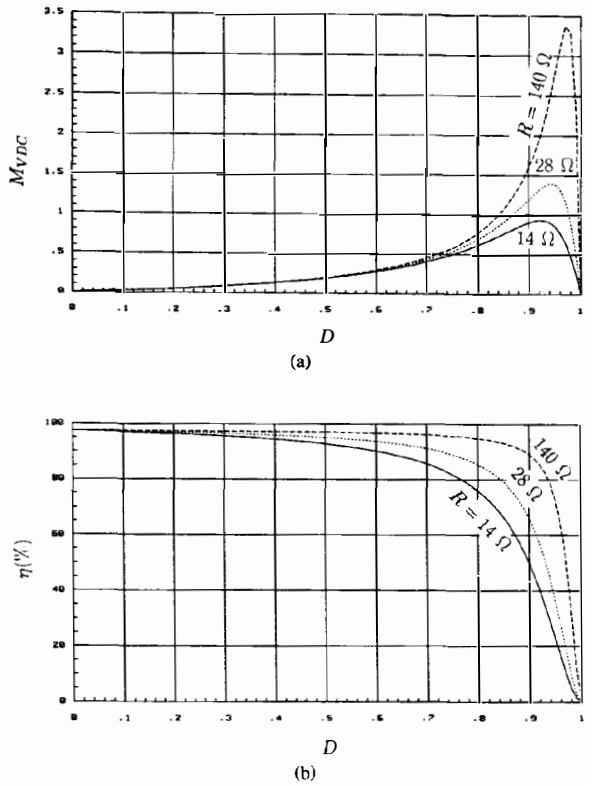

Fig. 4. Control-to-output transfer function $T_p = |T_p|e^{j\phi}$ for $n = 5$, $L = 1$ mH, $C = 47\ \mu$F, $R = 14\ \Omega$, $r_L = 2\ \Omega$, $r_{DS} = 0.5\ \Omega$, $r_{T1} = 50$ mΩ, $r_{T2} = 10$ mΩ, $R_F = 25$ mΩ, $r_C = 50$ mΩ, and $D = 0.1$ (solid line), 0.5, and 0.9. (a) $|T_p|$ against f. (b) ϕ against f.

$$\omega_{tl} = -\frac{1}{L}\left[\frac{n^2(1-D)^2R}{D^2} - r\right] \tag{29}$$

$$\xi_t = \frac{C\left\{r(R+r_C) + \dfrac{n^2(1-D)^2Rr_C}{D[n(1-D)+D]}\right\} + L}{2\sqrt{LC(R+r_C)\left\{r + \dfrac{n^2(1-D)^2R}{D[n(1-D)+D]}\right\}}} \tag{30}$$

$$\omega_t = \sqrt{\frac{r + \dfrac{n^2(1-D)^2R}{D[n(1-D)+D]}}{LC(R+r_C)}}. \tag{31}$$

Fig. 5 shows the magnitude and the phase of the control-to-output transfer function T_p as a function of frequency at $D = 0.1$, 0.5, and 0.9. The zero ω_{tl} is located either in the right half of the s-plane or the left half of the s-plane, depending upon the value of D for fixed resistances in the circuit. Therefore, the boost converter is a nonminimum phase system. As D increases from 0.9 to 1, the zero ω_{tl} is moved from the right half to the left half of s-plane. T_p has $\omega_{tl} = 0$ at $D \approx 0.9197$. The behavior of T_p when ω_{tl} crosses zero is illustrated in Fig. 5 for $D = 0.91965$, 0.9197, and 0.91975. For $D = 0.91965$ and 0.91975, plots of $|T_p|$ are identical and plots of ϕ differ at low frequencies by about 180°. Close examination reveals that, neglecting V_F in (25),

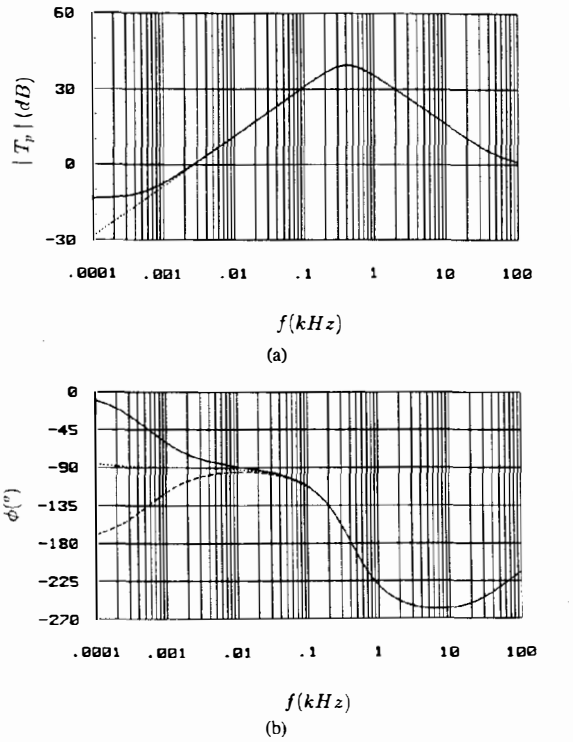

Fig. 5. Control-to-output transfer function $T_p = |T_p|e^{j\phi}$ for $n = 5$, $L = 1$ mH, $C = 47\ \mu$F, $R = 14\ \Omega$, $r_L = 2\ \Omega$, $r_{DS} = 0.5\ \Omega$, $r_{T1} = 50$ mΩ, $r_{T2} = 10$ mΩ, $R_F = 25$ mΩ, $r_C = 50$ mΩ, and $D = 0.91965$ (solid line), 0.9197, and 0.91975. (a) $|T_p|$ against f. (b) ϕ against f.

M_{VDC} reaches its maximum at the same value of D at which ω_{ti} crosses zero.

The *input-to-output voltage transfer function* (or the *audio susceptibility*) is

$$M_v(s) \equiv \left.\frac{v_o(s)}{v_i(s)}\right|_{d(s)=0} = \frac{n(1-D)Rr_C}{[n(1-D)+D]L(R+r_C)} \frac{s+\omega_{tc}}{s^2 + 2\xi_t\omega_t s + \omega_t^2}. \tag{32}$$

The input-to-output voltage transfer function M_v is illustrated in Fig. 6 for $D = 0.1$, 0.5, and 0.9.

The *open-loop input impedance* is

$$Z_i(s) \equiv \left.\frac{v_i(s)}{i_i(s)}\right|_{d(s)=0} = \frac{[n(1-D)+D]L}{D} \frac{s^2 + 2\xi_t\omega_t s + \omega_t^2}{s + \omega_{rc}} \tag{33}$$

where

$$\omega_{rc} = \frac{1}{C(R+r_C)}. \tag{34}$$

Fig. 7 shows the input impedance Z_i as a function of frequency for $D = 0.1$, 0.5, and 0.9.

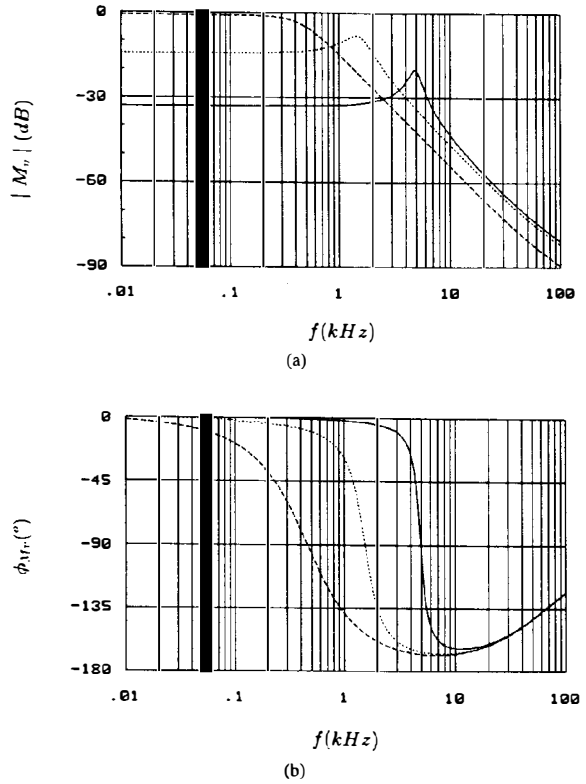

Fig. 6. Input-to-output transfer function $M_v = |M_v|e^{j\phi_{Mv}}$ for $n = 5$, $L = 1$ mH, $C = 47$ μF, $R = 14$ Ω, $r_L = 2$ Ω, $r_{DS} = 0.5$ Ω, $r_{T1} = 50$ mΩ, $r_{T2} = 10$ mΩ, $R_F = 25$ mΩ, $r_C = 50$ mΩ, and $D = 0.1$ (solid line), 0.5, and 0.9. (a) $|M_v|$ against f. (b) ϕ_{Mv} against f.

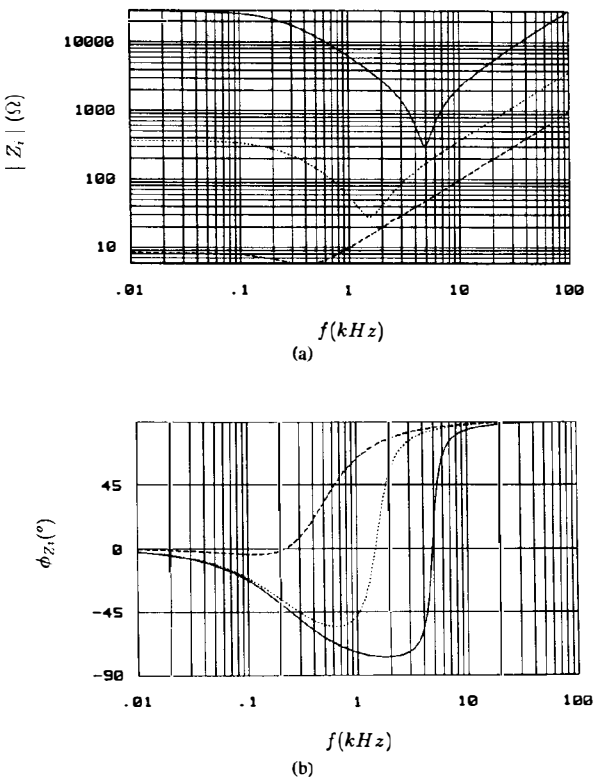

Fig. 7. Open-loop input impedance $Z_i = |Z_i|e^{j\phi_{Zi}}$ for $n = 5$, $L = 1$ mH, $C = 47$ μF, $R = 14$ Ω, $r_L = 2$ Ω, $r_{DS} = 0.5$ Ω, $r_{T1} = 50$ mΩ, $r_{T2} = 10$ mΩ, $R_F = 25$ mΩ, $r_C = 50$ mΩ, and $D = 0.1$ (solid line), 0.5, and 0.9. (a) $|Z_i|$ against f. (b) ϕ_{Zi} against f.

The *open-loop output impedance* is

$$Z_0(s) \equiv \frac{v_t(s)}{i_t(s)}\bigg|_{d(s)=0 \text{ and } v_i(s)=0} = \frac{Rr_C}{R + r_C}\,\frac{(s + \omega_{tc})(s + \omega_{ol})}{s^2 + 2\xi_t\omega_t s + \omega_t^2} \tag{35}$$

where

$$\omega_{ol} = \frac{r}{L}. \tag{36}$$

The output impedance Z_o is illustrated in Fig. 8 for $D = 0.1$, 0.5, and 0.9.

The low-frequency asymptotes are obtained by substituting $s = 0$ into the above expressions

$$T_p(0) = -\frac{V_O[D^2r - n^2(1 - D)^2R]}{D(1 - D)\{n^2(1 - D)^2R + D[n(1 - D) + D]r\}} \tag{37}$$

$$M_v(0) = \frac{nD(1 - D)R}{n^2(1 - D)^2R + D[n(1 - D) + D]r} \tag{38}$$

$$Z_i(0) = \frac{1}{D^2}\{n^2(1 - D)^2R + D[n(1 - D) + D]r\} \tag{39}$$

$$Z_0(0) = \frac{Rr}{r + \dfrac{n^2(1 - D)^2R}{D[n(1 - D) + D]}}. \tag{40}$$

Equation (38) is different from (25) because V_F has been assumed to be a short circuit for small-signal analysis.

All the models and expressions for the buck/boost converter can be obtained by substituting $n = 1$, $r_{T1} = 0$, and $r_{T2} = 0$. This is because the transformer is replaced by an inductor which is modeled by an inductance L and an ESR r_L.

V. Conclusions

A new method of modeling the PWM flyback and buck/boost converters operating in the continuous conduction mode has been introduced. In this method, the derivation of dc and small-signal models begins from the static voltage and current transfer functions of the idealized switching part of the converter. Next, both transfer functions are perturbed and linearized at the operating point. Finally, the equivalent averaged resistances of switched resistances are determined using the principle of energy conservation. This procedure leads to pure circuit models consisting of standard components. An important advantage of the models is that they can be used in circuit-simulation programs such as SPICE. Using the new models, the dc voltage transfer function, the efficiency, and small-signal characteristics have been derived, taking into account all parasitic resistances of the converters. In most previous papers, the ON

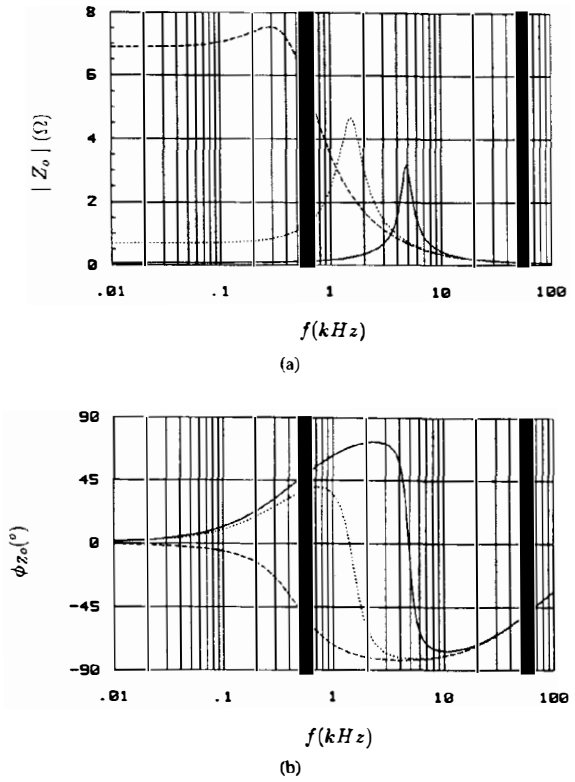

Fig. 8. Open-loop output impedance $Z_o = |Z_o|e^{j\phi_{Zo}}$ for $n = 5$, $L = 1$ mH, $C = 47$ μF, $R = 14$ Ω, $r_L = 2$ Ω, $r_{DS} = 0.5$ Ω, $r_{T1} = 50$ mΩ, $r_{T2} = 10$ mΩ, $R_F = 25$ mΩ, $r_C = 50$ mΩ, and $D = 0.1$ (solid line), 0.5, and 0.9. (a) $|Z_o|$ against f. (b) ϕ_{Zo} against f.

resistances of the switch and the diode, and the threshold voltage of the diode have been neglected. The effects of the duty ratio on the dc and small-signal characteristics are illustrated. It is shown that one of the zeros of the control-to-output transfer function moves from the right half of the s-plane to the left half of the s-plane as the duty ratio approaches 1. In this case, the phase of the control-to-output function changes from 0° to −180° at low frequencies. Although not shown, effects of the load resistance, and of the parasitic resistances, were also examined. The load resistance influences significantly all of the dynamic characteristics except the input-to-output transfer function. Variations of the EAR in series with the inductor affects only the output impedance at low frequencies. The ESR of the capacitor influences the converter dynamic characteristis at high frequencies. The dc and small-signal characteristics derived from the introduced circuit models are the same as those obtained from the state-space averaging method. Experimental results validating these characteristics are given in [1]. The proposed linear circuit models are suitable for modeling and analyzing small-signal operation of PWM converters at a given operating point. Large-signal dynamic behavior of the converters should be described using nonlinear techniques [10].

Appendix

A power stage of a PWM flyback converter shown in Fig. 1(a) will be designed to meet the following specifications: continuous conduction mode, $V_I = 240$ to 300 V, $V_O = 28$ V, $I_O = 0.2$ to 2 A, $f_s = 200$ kHz, $V_r/V_O \le 1\%$, where V_r is the maximum peak-to-peak value of the ripple voltage on the dc output voltage.

The minimum and maximum values of the load resistance are $R_{\min} = V_O/I_{O\max} = 14$ Ω and $R_{\max} = V_O/I_{O\min} = 140$ Ω, respectively. Let us assume $n = 5$. From (25), $D_{\max} \approx 0.38$ and $D_{\min} \approx 0.32$. From the condition for continuous conduction mode,

$$L_{\min} = \frac{nR_{\max}}{2fs}(1 - D_{\min})^2 = 809.2\ \mu\text{H; let } L = 1\ \text{mH}. \quad \text{(A1)}$$

The maximum allowable value of the peak-to-peak ripple voltage is $V_r = V_O/100 = 280$ mV. The maximum value of the peak diode current $I_{DM\max} = I_{O\max}/(1 - D_{\max}) = 3.23$ A. Assuming the ESR of the filter capacitor $r_C = 50$ mΩ, the maximum value of the peak-to-peak voltage across the ESR is $V_{rc} = r_C I_{DM\max} = 50 \times 3.23 = 161$ mV. Thus, the maximum permissible value of the peak-to-peak voltage across the filter capacitance C is $V_{C\max} = V_r - V_{rc} = 280 - 161 = 119$ mV. The minimum value of the filter capacitance is found as

$$C_{\min} = \frac{I_{O\max} D_{\max}}{f_s V_{C\max}} = 31.9\ \mu\text{F; let C} = 47\ \mu\text{F}. \quad \text{(A2)}$$

References

[1] R. D. Middlebrook and S. Cuk, *Advances in Switched-Mode Power Conversion*, vols I and II. Pasadena, CA: TESLAco, 1981, pp. 73–89.

[2] R. P. Severns and G. Bloom, *Modern DC-to-DC Switchmode Power Converter Circuits*. New York: Van Nostrand, 1985.

[3] D. M. Mitchell, *Switching Regulator Analysis*. New York: McGraw-Hill, 1988.

[4] N. Mohan, T. M. Undeland, and W. P. Robbins, *Power Electronics: Converters, Applications and Design*. New York: Wiley, 1989, pp. 81–87, 214–217, and 237–239.

[5] A. Kislovski, R. Redl, and N. O. Sokal, *Analysis of Switching-Mode DC / DC Converters*. New York: Van Nostrand, 1991.

[6] Y. S. Lee, "A systematic and unified approach to modeling switches in switch-mode power supplies," *IEEE Trans. Ind. Electron.*, vol. IE-32, pp. 445–448, Nov. 1985.

[7] V. Vorpérian, "Simplified analysis of PWM converters using the model of the PWM switch, Part I: Continuous conduction mode," *IEEE Trans. Aerosp. Electron. Syst.*, vol. 26, pp. 497–505, May 1990.

[8] H. J. Sira-Ramirez, "Switched control of bilinear converters via pseudolinearization," *IEEE Trans. Circuits Syst.*, vol. CAS-36, pp. 858–865, June 1989.

[9] ——, "Nonlinear P-I controller design for switchmode dc-to-dc power converters," *IEEE Trans. Circuits Syst.*, vol. CAS-38, pp. 410–417, Apr. 1991.

[10] H. Sira-Ramirez and P. Lischinsky-Arenas, "Differential algebraic approach in non-linear dynamical compensator design for d.c.-to-d.c. power converters," *Int. J. Contr.*, vol. 54, pp. 111–133, July 1991.